Scorpion β-toxin interference with Na_V channel voltage sensor gives rise to excitatory and depressant modes

Enrico Leipold,[1] Adolfo Borges,[2] and Stefan H. Heinemann[1]

[1]Department of Biophysics, Center for Molecular Biomedicine, Friedrich Schiller University of Jena and Jena University Hospital, Jena D-07745, Germany

[2]Laboratorio de Biología Molecular de Toxinas y Receptores, Instituto de Medicina Experimental, Universidad Central de Venezuela, Caracas 1050-A, Venezuela

Scorpion β toxins, peptides of ∼70 residues, specifically target voltage-gated sodium (Na_V) channels to cause use-dependent subthreshold channel openings via a voltage–sensor trapping mechanism. This excitatory action is often overlaid by a not yet understood depressant mode in which Na_V channel activity is inhibited. Here, we analyzed these two modes of gating modification by β-toxin Tz1 from *Tityus zulianus* on heterologously expressed $Na_V1.4$ and $Na_V1.5$ channels using the whole cell patch-clamp method. Tz1 facilitated the opening of $Na_V1.4$ in a use-dependent manner and inhibited channel opening with a reversed use dependence. In contrast, the opening of $Na_V1.5$ was exclusively inhibited without noticeable use dependence. Using chimeras of $Na_V1.4$ and $Na_V1.5$ channels, we demonstrated that gating modification by Tz1 depends on the specific structure of the voltage sensor in domain 2. Although residue G658 in $Na_V1.4$ promotes the use-dependent transitions between Tz1 modification phenotypes, the equivalent residue in $Na_V1.5$, N803, abolishes them. Gating charge neutralizations in the $Na_V1.4$ domain 2 voltage sensor identified arginine residues at positions 663 and 669 as crucial for the outward and inward movement of this sensor, respectively. Our data support a model in which Tz1 can stabilize two conformations of the domain 2 voltage sensor: a preactivated outward position leading to Na_V channels that open at subthreshold potentials, and a deactivated inward position preventing channels from opening. The results are best explained by a two-state voltage–sensor trapping model in that bound scorpion β toxin slows the activation as well as the deactivation kinetics of the voltage sensor in domain 2.

The Journal of General Physiology

INTRODUCTION

Voltage-gated sodium (Na_V) channels are membrane proteins, which initiate and propagate action potentials and therefore play a major role in the electrical communication of excitable cells (Catterall, 2000). Na_V channel complexes consist of a large pore-forming α subunit (∼260 kD) and up to two smaller auxiliary β subunits. The α subunit has a pseudo-tetrameric structure; it is composed of four homologous domains, each with six transmembrane segments (S1–S6) connected by extra and intracellular loops. Segments S5 and S6 of each domain arrange around a central pore, and the hairpin-like pore loops connecting S5 and S6 form the channels' selectivity filter (Heinemann et al., 1992). Segments S1–S4 of each domain serve as voltage sensors, with the positive gating charges located in the S4 segments. These voltage sensors move outward upon membrane depolarization and initiate the voltage-dependent activation and inactivation of Na_V channels (Yang and Horn, 1995; Yang et al., 1996, 1997; Cha et al., 1999; DeCaen et al., 2008).

Scorpion venoms contain two classes of long-chain peptide toxins (60–76 residues), α toxins and β toxins, which efficiently disturb neuronal excitation by modulating the function of Na_V channels (Catterall et al., 1992; Gordon, 1997). Scorpion α toxins bind to receptor site 3 on Na_V channels to impair rapid channel inactivation, whereas scorpion β toxins bind to receptor site 4 and show rather complex effects. On the one hand, they induce spontaneous and repetitive firing of action potentials by permitting Na_V channels to activate at subthreshold membrane potentials. On the other hand, they reduce the peak Na_V channel current (de la Vega and Possani, 2007; Catterall et al., 2007). Thus, it appears that scorpion β toxins have a bimodal function because they can enhance ("excitatory mode") and inhibit ("depressant mode") the activity of Na_V channels and hence the excitability of neurons. Furthermore, β toxins are subtype specific, as they discriminate between different Na_V channel isoforms (e.g., Cestèle et al., 1998; Borges et al., 2004; Leipold et al., 2006; Vandendriessche et al., 2010). Accordingly, the physiological consequences of a certain β toxin are hard to predict because they may depend not

Correspondence to Stefan H. Heinemann: stefan.h.heinemann@uni-jena.de

Abbreviations used in this paper: BmK, *Buthus martensii Karsch*; LY, Lucifer yellow; Na_V, voltage-gated sodium.

The Rockefeller University Press $30.00
J. Gen. Physiol. Vol. 139 No. 4 305–319
www.jgp.org/cgi/doi/10.1085/jgp.201110720

only on the dominant mode of the toxin but also on the affected channel subtypes.

Several β toxins are classified as either "excitatory" or "depressant" toxins based on their effects on neuronal excitation in insects. Typical excitatory β toxins like AaH IT_1 and AaH IT_2 (*Androctonus australis hector*; Loret et al., 1990), Lqq IT_1 (*Leiurus quinquestriatus quinquestriatus*; Zlotkin et al., 1985), or Bj-xtrIT (*Buthotus judaicus*; Oren et al., 1998) cause fast contraction paralysis in insects, whereas depressant β toxins like Lqq IT_2 (*Leiurus quinquestriatus quinquestriatus*; Zlotkin et al., 1985; Bosmans et al., 2005) or Lqh IT_2 (*Leiurus quinquestriatus hebraeus*; Zlotkin et al., 1993) lead to a progressive flaccid paralysis by inhibiting neuromuscular transmission.

Although increased neuronal excitability typically is an unwanted effect, β toxins recently attracted attention because some members isolated from the venom of *Buthus martensii Karsch* (BmK) show antinociceptive effects in mammals by depressing neuronal excitation. BmK $AngP_1$, for example, has an analgesic effect in mice when injected intravenously (Guan et al., 2001). BmK IT_2 (Li et al., 2000; Wang et al., 2000; Tan et al., 2001b; Zhang et al., 2003; Bai et al., 2007) and BmK AS (Tan et al., 2001a; Chen and Ji, 2002; Chen et al., 2006; Liu et al., 2008) are analgesics in rat pain models, as they inhibit Na_V channels in the periphery and in DRG neurons. The molecular mechanism underlying the specific inhibition of Na_V channels by these peptides, however, is unknown so far.

Previous studies on the molecular mechanism of β toxins concentrated on their excitatory effect, i.e., their ability to open Na_V channels at resting voltage by left-shifting the voltage dependence of channel activation. This effect is use dependent because the activation shift is enhanced when channels are preactivated with a depolarizing prepulse. Cestèle et al. (1998) compared the effects of CssIV (from *Centruroides suffusus suffusus*) on brain-type $Na_V1.2$ and heart-type $Na_V1.5$ channels and found remarkable differences. CssIV left-shifted the activation of $Na_V1.2$ in a prepulse-dependent manner and slightly decreased the current amplitude of $Na_V1.2$. In contrast, CssIV inhibited $Na_V1.5$ independently of a prepulse. They identified glycine residue G845 in the S3/S4 linker of the voltage sensor in domain 2 of $Na_V1.2$ as critical for the effect of CssIV to left-shift the voltage dependence of activation. This glycine is conserved among most Na_V channels, but $Na_V1.5$ harbors an asparagine at the homologous position. Mutation of glycine to asparagine (G845N) conferred a $Na_V1.5$-like phenotype to $Na_V1.2$. A voltage–sensor trapping model was proposed in which CssIV reduces the activation energy necessary for channel opening by arresting the voltage sensor of domain 2 in an activated position (Cestèle et al., 1998, 2001; Mantegazza and Cestèle, 2005; Catterall et al., 2007).

Recently, we reported that β-toxin Tz1, the main long-chain toxin produced by the Venezuelan scorpion *Tityus zulianus*, is in many respects similar to CssIV; it left-shifts the activation of $Na_V1.4$ in a use-dependent manner but inhibits $Na_V1.5$ channels independent of a prepulse (Borges et al., 2004). We further demonstrated the relevance of the conserved glycine (G658 in $Na_V1.4$) for the mechanism of Tz1 to left-shift the voltage dependence of $Na_V1.4$ activation (Leipold et al., 2006), suggesting a general importance of this residue for the action of β toxins. In addition, we identified a second interaction site for Tz1 located in the pore loop of domain 3 that determines the specificity of Na_V channels toward Tz1 (Leipold et al., 2006). The interaction epitopes identified in these studies, the S3/S4 linker in the voltage sensor of domain 2 and the pore loop in domain 3, are expected to be in close proximity and thus may be part of receptor site 4, the binding site for β toxins on the channel surface.

Although the voltage–sensor trapping model by Cestèle et al. (1998) explains the enhanced activation of Na_V channels by β toxins (excitatory effect), it provides no satisfying explanation for the tendency of β toxins to simultaneously inhibit Na_V channels (depressant effect). We therefore investigated systematically and quantitatively how Tz1 modulates Na_V channels. Our data support a model in which Tz1 stabilizes two conformations of the voltage sensor in domain 2 of Na_V channels: an activated outward conformation corresponding to "enhanced channel activation," and a resting conformation corresponding to "channel inhibition" in which channels are prevented from opening. Furthermore, we provide information on the movement of the voltage sensor in domain 2 of Na_V channels in the presence of β toxins.

MATERIALS AND METHODS

Channel constructs

The wild-type channels used in this study were the rat skeletal muscle sodium channel $Na_V1.4$ (SCN4A and M26643.1; Trimmer et al., 1989) and the human heart sodium channel $Na_V1.5$ (SCN5A and Q14524; Gellens et al., 1992). $Na_V1.4$ mutant 44p(1.7)4 (Leipold et al., 2006) contains the domain 3 pore loop region of human $Na_V1.7$, which combines the following amino acid substitutions: R1250V, E1251N, K1252V, E1253D, E1254K, H1257K, V1260Y, and N1261S. Construction of $Na_V1.4$ mutant channels G658N (Leipold et al., 2006), R663C, and R666C (Leipold et al., 2007) was described previously. $Na_V1.4$ mutant channels R669C, K672C, K675C, 44p(1.7)4-G658N, IFC (M1305C), IFC-G658N, as well as $Na_V1.5$-N803G were produced using a PCR-based strategy. All mutations were verified by sequencing. Plasmid DNA was isolated from *Escherichia coli* using the Midi-Plasmid Purification kit (QIAGEN).

Cell culture and transfection

HEK 293 cells (Centre for Applied Microbiology and Research) were maintained in 45% Dulbecco's modified Eagle's medium and 45% Ham's F12 medium, supplemented with 10% fetal calf serum in a 5% CO_2 incubator at 37°C. HEK 293 cells were trypsinized, diluted with culture medium, and grown in 35-mm dishes. When grown to 30–50% confluence, cells were transfected with the Na_V channel expression plasmids. Electrophysiological recordings were performed 2–3 d after transfection.

Solutions and toxin

The patch pipettes contained (in mM): 35 NaCl, 105 CsF, 10 EGTA, and 10 HEPES, pH 7.4 with CsOH. The bath solution contained (in mM): 150 NaCl, 2 KCl, 1.5 $CaCl_2$, 1 $MgCl_2$, and 10 HEPES, pH 7.4 with NaOH. Scorpion β-toxin Tz1 was obtained from *T. zulianus* crude venom, according to a procedure described previously (Borges et al., 2004). The toxin was diluted in bath solution containing 1 mg/ml BSA and stored at −20°C until use. Tz1 was locally applied with a glass pipette, as described previously (Chen et al., 2000).

Fast inactivation of channel mutant IFC was removed with 200 µM Lucifer yellow (LY; Sigma-Aldrich) in the pipette and illuminating it with light from a mercury epifluorescent lamp using a 450–490-nm excitation filter (Heinemann and Leipold, 2011). Control experiments showing that LY did not alter the voltage-dependent activation behavior of $Na_V1.4$, $Na_V1.4$-IFC, and $Na_V1.4$-IFC-G658N are shown in Fig. S4.

Electrophysiology

Whole cell voltage-clamp experiments were performed as described previously (Chen et al., 2000). Patch pipettes had resistances of 0.9–1.5 MΩ, and the series resistance was compensated for by >70% to minimize voltage errors. Only cells with series resistances <3.5 MΩ were used. An EPC-10 patch-clamp amplifier was operated by PatchMaster software (both from HEKA). Leak and capacitive currents were corrected with a p/6 method. Currents were low-pass filtered at 5 kHz and sampled at a rate of 25 kHz. All experiments were performed at constant temperature (19–21°C). Data analysis was performed using IgorPro (WaveMetrics) and FitMaster software (HEKA). All data were presented as mean ± SEM (n = number of independent experiments). Datasets were tested for statistical significance using Student's t test with unequal variances when appropriate.

Action potential–like stimulations. Action potential–like stimulations were approximated with a three-step voltage ramp protocol. From a holding potential of −160 mV, a first 1-ms voltage ramp to −70 mV followed by a second 0.5-ms ramp to 20 mV and a third 2-ms ramp to −160 mV were applied at frequencies of 0.1 or 2 Hz.

Current–voltage relationships. From a holding potential of −160 mV, cells were depolarized with a three-step protocol (see Fig. 2 A). The first and the last depolarization of 20-ms duration ranged from −110 to 60 mV in steps of 10 mV. The central pulse to −10 mV for 50 ms was used as a prepulse to prime the channels. The segments of 50 ms at −160 mV before and after the prepulse ensured recovery from inactivation. The peak currents during the first and third depolarization were plotted as a function of voltage, yielding two current–voltage relationships: one without and one with prepulse. The repetition interval was 30 s. For a quantitative data description, the current–voltage relationships in absence and presence of Tz1 were analyzed using a global fit procedure according to a Hodgkin–Huxley formalism:

$$I(V) = P_o(V)\,\Gamma_{\max}\,V\frac{1-e^{-(V-E_{rev})/25\,mV}}{1-e^{-V/25\,mV}} \quad (1)$$

$$P_o(V) = \frac{1-P_{tox}}{\left(1+e^{-(V-V_m)/k_m}\right)^3} + \frac{P_a}{\left(1+e^{-(V-V_m-\Delta V_a)/k_m}\right)^2} + \frac{P_i}{\left(1+e^{-(V-V_m-\Delta V_i)/k_i}\right)^1}$$

$$P_{tox} = P_a + P_i,$$

where I is the peak test pulse current and V is the test pulse voltage. E_{rev} is the reversal potential, and G_{max} is the maximal conductance of all channels. Open probabilities (P_o) were described with a triple Boltzmann formalism assuming two fractions of Tz1-modified channels: one fraction of channels with enhanced activation (P_a), and a second fraction of channels with strongly inhibited activation (P_i). V_m is the voltage of half-maximal gate activation, and k_m is the corresponding slope factor when channels have no Tz1 bound. ΔV_a and ΔV_i represent the voltages by which Tz1 shifts the activation of preactivated and inhibited channels, respectively. k_i is the slope factor associated with ΔV_i. Toxin-bound channels with enhanced activation are assumed to activate with two independent gates, as one is trapped in an activated position. Toxin-bound channels with strongly inhibited activation are assumed to activate with only one gate, as Tz1 is assumed to limit the activation of a fraction of channels by trapping this gate in its resting conformation, ultimately preventing channel opening. P_{tox} is the sum of P_a and P_i and represents the probability of the channels to have Tz1 bound. Current–voltage relations before and after Tz1 application were simultaneously fit with a unique set of E_{rev}, V_m, k_m, ΔV_a, ΔV_i, and k_i values. Fits were further constrained in the following manner: (a) P_a and P_i in the absence of Tz1 were set to zero, which means describing the activation of channels with a Hodgkin–Huxley formalism involving $m = 3$ activation gates and single-channel characteristics according to Goldman, Hodgkin, and Katz; (b) for $Na_V1.4$ and $Na_V1.5$-N803G, P_{tox} was considered independent of a prepulse; and (c) in the presence of Tz1, P_a was set to zero for $Na_V1.5$ and $Na_V1.4$-G658N because these channels are exclusively inhibited by Tz1.

Steady-state inactivation. From a holding potential of −160 mV, cells were conditioned for 500 ms at voltages ranging from −160 to −30 mV in steps of 10 mV. Subsequently, peak current was determined at −20 mV. The repetition interval was 20 s. The peak current plotted versus the conditioning voltage was described with a Boltzmann function:

$$I(V) = I_0 + \frac{I_{\min}}{1+e^{-(V-V_h)/k_h}}, \quad (2)$$

with the half-maximal inactivation voltage V_h and the corresponding slope factor k_h indicating the voltage dependence of steady-state fast inactivation.

Concentration–response analysis. P_{tox}, obtained from current–voltage relationships (Eq. 1), was plotted as a function of the Tz1 concentration and described with the Hill equation:

$$P_{tox} = P_{\max}\Big/\left(1+\frac{EC_{50}}{[Tz1]}\right)^h, \quad (3)$$

where h is the Hill coefficient, [Tz1] is the Tz1 concentration, and P_{max} is the maximally obtained value for P_{tox}. EC_{50} is the Tz1 concentration, where P_{tox} becomes half-maximal. P_a and P_i (see Eq. 1) were described with the same equation assuming identical EC_{50} values for P_{tox}, P_a, and P_i. Errors of EC_{50} values were obtained from the data fits using IgorPro software.

Nonstationary noise analysis. From a holding potential of −160 mV, cells were conditioned with a 50-ms prepulse to 20 mV, and subsequently, a train of 20-ms test depolarizations to −70, −40, −10, and 20 mV, with 40-ms repolarization steps to −160 mV between the individual depolarizations, was applied 50–200 times in the absence and presence of 5 µM Tz1. The leak-corrected mean current response and the variance of successive records were calculated for each test depolarization using PulseTools software (HEKA). Variance was plotted as a function of the mean current and analyzed assuming a binomial distribution of channel states (Sigworth, 1977):

$$\sigma^2 = \sigma_b^2 + \left(i\cdot I - \frac{I^2}{N}\right), \quad (4)$$

where σ^2 is the variance, σ_b^2 is the background variance, and I is the macroscopic mean current response of all individual test depolarizations. N defines the number of channels underlying the macroscopic current, and i is an estimate for the single-channel current. The maximal open probability P_o was estimated from the variance analysis according to:

$$P_o = \frac{I_{max}}{i \cdot N}. \quad (5)$$

To reduce the number of independent variables and to constrain the number of active channels even for data obtained at voltages yielding low open probabilities, variance–current curves for all available test voltages were fit simultaneously according to Starkus et al. (2003). Furthermore, in the presence of Tz1, N was set to the value obtained under control conditions. Variance–current fits at −70 mV were constrained to $N * P_a$, where P_a is the fraction of channels with a left-shifted activation obtained from Eq. 1.

Voltage-dependent activation. From a holding potential of −160 mV, the current amplitude at −70 mV (I_a; Fig. 8 A) was measured with a 20-ms test pulse in the presence of 25 µM Tz1 100 ms after conditioning pulses of various lengths. The conditioning voltages were −20, −40, and −60 mV, and the repetition interval was 30 s. Normalized I_a was plotted as a function of the conditioning duration, and the kinetics of the depolarization-induced preactivation of toxin-modified channels was analyzed with a single-exponential function yielding an activation time constant τ_a.

Voltage-dependent deactivation. From a holding potential of −160 mV, the current amplitude at −70 mV (I_{max}; Fig. 8 B) was measured with a 20-ms test pulse after priming the channels with a series of two 50-ms depolarizations to −10 mV in the presence of 25 µM Tz1. Subsequently, conditioning pulses of various lengths were applied, followed by a second 20-ms test pulse at −70 mV (I_d). Repolarization to −160 mV for 50 ms between depolarizations and before and after conditioning ensured recovery from fast inactivation. The conditioning voltages were −120, −140, −160, and −180 mV, and the repetition interval was 30 s. The ratio I_d/I_{max}, the probability of channels not being deactivated after conditioning, was plotted as a function of the conditioning duration and described with a single-exponential function yielding a deactivation time constant τ_d.

Voltage dependence of Tz1 effects. Activation and deactivation time constants in the presence of Tz1, plotted as a function of conditioning voltage, were fit with an transition-state model providing an estimate of the effective charge transfer, q, during the voltage-dependent activation and deactivation of Tz1-bound channels and a symmetry factor, δ, estimating the gating charge fraction involved in the deactivation process of the sensor:

$$\tau(V) = \frac{\tau_{max}}{e^{(V-V_0)(1-\delta)q/kT} + e^{-(V-V_0)\delta q/kT}}. \quad (6)$$

τ_{max} is the time constant of the transition between the activated and the resting state of the channels at the equilibrium voltage V_0. T is the absolute temperature, and k is the Boltzmann constant.

Online supplemental material

Dependence of Tz1 effects on stimulation frequency is presented in Fig. S1. Conductance–voltage analyses for $Na_V1.4$, $Na_V1.5$, $Na_V1.4$-G658N, and $Na_V1.5$-N803G are shown in Fig. S2. Voltage dependencies of steady-state inactivation for $Na_V1.4$, $Na_V1.5$, mutants $Na_V1.4$-G658N, $Na_V1.5$-N803G, 44(p1.7)4, and 44(p1.7)4-G658N are shown in Fig. S3, and for domain 2 charge neutralization mutants in Fig. S6. Fig. S4 illustrates the effects of LY on channel gating, and Fig. S5 contains current traces of inactivation-deficient $Na_V1.4$-IFC and $Na_V1.4$-IFC-G658N channels. Nonstationary noise analysis of inactivation-deficient $Na_V1.4$-IFC channels is presented in Fig. S7, and further examples of variance–voltage analyses are shown in Fig. S8. Time courses of Tz1-induced gating transitions of charge neutralization mutants are shown in Fig. S9. Table S1 holds information on the voltage dependence of activation and inactivation of all Na_V channels and mutants used. The online supplemental material is available at http://www.jgp.org/cgi/content/full/jgp.201110720/DC1.

RESULTS

Excitatory and depressant action of Tz1

Using the whole cell patch-clamp technique on HEK 293 cells transiently expressing the channel subtypes $Na_V1.4$ (skeletal muscle) or $Na_V1.5$ (cardiac muscle), we investigated the functional impact of scorpion β-toxin Tz1, the main component in the venom of *T. zulianus*. To test for the excitatory and depressant potency of Tz1, we applied trains of 20 action potential–like voltage pulses at frequencies of 0.1 and 2 Hz, as indicated in Fig. 1 A, in the absence and presence of 5 µM Tz1. At a stimulation frequency of 0.1 Hz, Tz1 reduced the Na^+ current through $Na_V1.4$ channels, whereas it was increased when stimulation was performed at 2 Hz (Fig. 1 B, left). In contrast, Tz1 reduced the current amplitudes of $Na_V1.5$ at both stimulation frequencies (Fig. 1 B, right). Analysis of current integrals (Fig. 1 B, gray areas) provided an operational measure of channel activity and gave an indication of the amount of Na^+ influx during a single action potential. At 0.1-Hz stimulation, the application of Tz1 reduced the current integral of $Na_V1.4$ in the last of 20 stimulations to 81.5 ± 1.2%, whereas the integrals increased to 155.6 ± 6.6% (n = 5) for 2-Hz stimulation (Fig. 1 C, top). This use-dependent alteration of current integrals was fully reversible and also occurred for prolonged stimulation periods (Fig. S1). This illustrates the bimodal functionality of Tz1 for $Na_V1.4$ channels as a "depressant toxin" at low stimulation frequencies and an "excitatory toxin" at higher frequencies. Tz1 reduced the activity of $Na_V1.5$ channels to 80.8 ± 1.6% (n = 7) independently of the stimulation frequency (Fig. 1, B, right, and C, bottom).

Glycine 658 in $Na_V1.4$ determines the mode of Tz1 action

In a recent study (Leipold et al., 2006), we showed that mutation of $Na_V1.4$ channels at that site (G658N) eliminated the ability of Tz1 to induce a negative shift in the voltage dependence of activation, much like what was shown for $Na_V1.2$ channels and CssIV (Cestèle et al., 1998). To gain insight into the molecular mechanisms underlying the two modes of Tz1 action, we measured and quantitatively described the effects of Tz1 on the voltage dependence of activation of $Na_V1.4$, $Na_V1.4$-G658N, $Na_V1.5$, and the reverse mutant channel $Na_V1.5$-N803G.

Current–voltage relationships were measured in a three-pulse protocol (Fig. 2 A) to infer about channel activation from resting conditions (IV1) and after preactivation by a 50-ms pulse to −10 mV (IV2). The priming prepulse facilitates toxin-induced trapping of the voltage sensor in domain 2 in an activated position. Although $Na_V1.4$ channels started to activate at about −50 mV under control conditions (Fig. 2 B, open circles), channel opening started to occur at −90 mV in a prepulse-dependent manner in the presence of 5 µM Tz1: after prepulse application, the current amplitudes in IV2 were much larger than in IV1 (Fig. 2 B, closed symbols). However, in addition to the use-dependent facilitation of $Na_V1.4$ activation, inhibition of the peak current amplitudes occurred at stronger depolarizations with a negative use dependence; i.e., current inhibition was stronger without a prepulse.

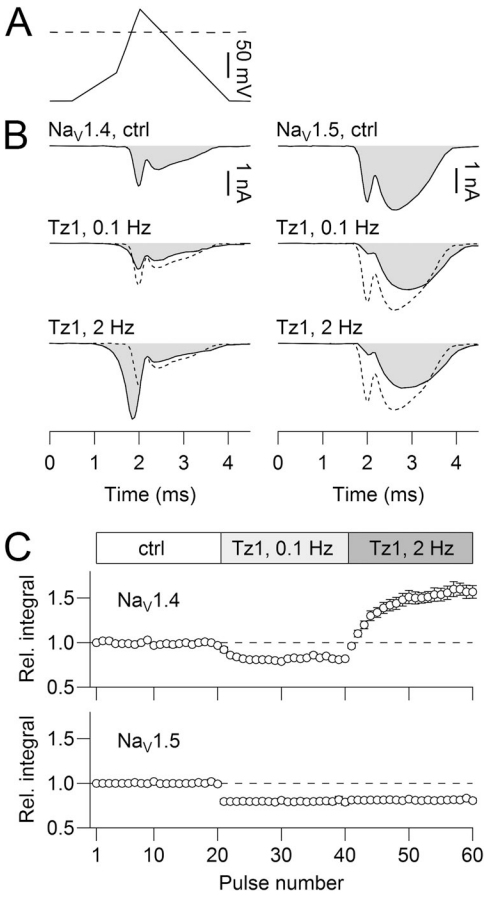

Figure 1. Scorpion β-toxin Tz1 enhances or inhibits the activity of Na_V channels in a subtype-specific and use-dependent manner. (A) Action potential–like voltage protocol used to elicit current responses from HEK 293 cells transiently expressing $Na_V1.4$ or $Na_V1.5$ channels. Successive trains of 20 individual pulses were applied at frequencies of 0.1 and 2 Hz. (B) Representative current traces of $Na_V1.4$ (left) and $Na_V1.5$ (right) channels, each obtained from the last stimulation of a train of 20 pulses before (ctrl) and after the application of 5 µM Tz1 (Tz1) for the indicated stimulation frequencies. Gray shaded areas visualize current integrals, and dashed lines indicate current responses under control conditions. (C) Mean integrals for $Na_V1.4$ ($n = 5$) and $Na_V1.5$ ($n = 7$) in the absence (ctrl) and presence of Tz1, normalized to the integrals under control conditions as a function of the pulse number. Horizontal bars indicate stimulation frequencies and the presence of 5 µM Tz1.

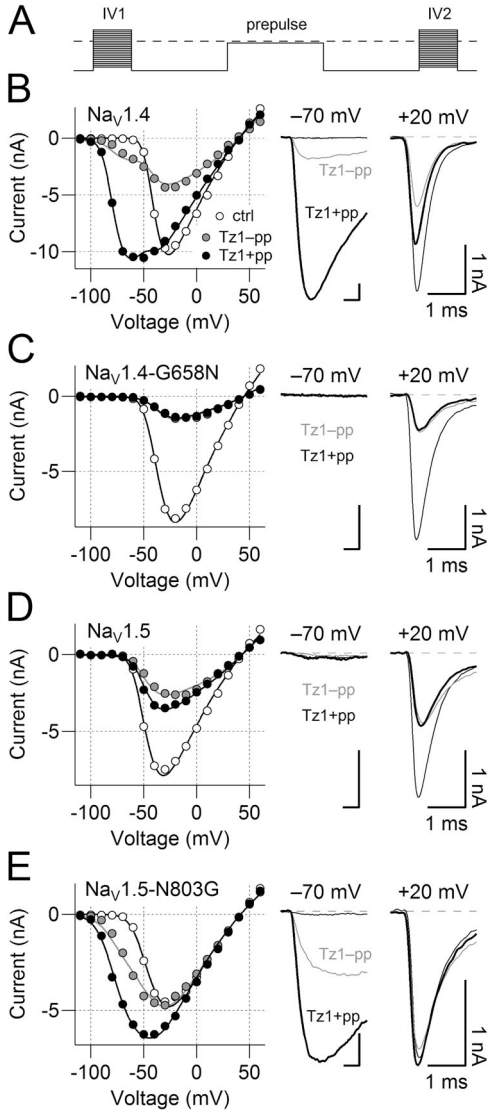

Figure 2. The domain 2 S3/S4 linker determines how Tz1 modifies Na_V channel gating. (A) Pulse protocol used to elicit currents at potentials ranging from −110 to 60 mV in steps of 10 mV. IV1 denotes a first series of test potentials, and IV2 is a second test potential series applied after a 50-ms conditioning prepulse to −10 mV. (B–E; left) Representative current–voltage plots before (open circles) and after the application of 5 µM Tz1 (closed symbols) without (gray) or with (black) a preceding prepulse. Control data are shown without a prepulse, as they are indistinguishable from those with a prepulse. Continuous curves are data fits according to Eq. 1. (Right) Current traces from the same experiments as shown on the left obtained at the indicated potentials in the absence (thin black) and presence of Tz1 without (gray) and with (thick black) a prepulse. Experiments were performed for $Na_V1.4$ (B), $Na_V1.4$–G658N (C), $Na_V1.5$ (D), and $Na_V1.5$–N803G (E).

Current–voltage relationships were analyzed quantitatively according to a Hodgkin–Huxley model of channel activation (Eq. 1). This formalism splits the channel population into three components: one of "control" channels without bound Tz1 ($1 - P_{tox}$), one fraction of channels showing Tz1-facilitated activation (P_a), and another one in which channel activation is inhibited by Tz1 (P_i). Fitting this model to the activation behavior of $Na_V1.4$ in the presence of 5 µM Tz1 (Fig. 2 B) revealed a P_{tox} value of 0.66 ± 0.09 ($n = 5$), indicating that Tz1 affected more than half of the channel population under this condition. P_{tox} values were found to be independent of a prepulse; i.e., the toxin apparently does not separate from the channel during the applied pulse paradigm.

The channel fraction with Tz1-facilitated activation, P_a, increased from 0.05 ± 0.02 before to 0.44 ± 0.05 after the prepulse and displayed a prepulse-independent shift of the half-maximal activation voltage, ΔV_a, of −35.2 ± 1.5 mV. Likewise, the channel fraction inhibited by Tz1, P_i, decreased from 0.61 ± 0.07 to 0.23 ± 0.05 and displayed a prepulse-independent shift of the half-maximal activation voltage, ΔV_i, of 56.0 ± 9.3 mV. Thus, channel priming redistributes $Na_V1.4$ channels between the phenotypes "activated by Tz1" and "inhibited by Tz1" by influencing the voltage dependence of the channel's activation process. The concentration dependencies of both toxin phenotypes were analyzed assuming a prepulse-independent 1:1 binding of Tz1. For $Na_V1.4$ (Fig. 3 A), the maximal values of P_a and P_i in the absence of a prepulse were 0.09 ± 0.01 and 0.83 ± 0.01, respectively, highlighting "inhibited by Tz1" as the dominant phenotype. In presence of a prepulse, the values changed to 0.51 ± 0.06 for P_a and to 0.41 ± 0.04 for P_i, indicating that "activated by Tz1" dominated under this condition. The half-maximal concentrations of P_{tox}, P_a, and P_i were identical (2.7 ± 0.5 µM), suggesting that both Tz1 phenotypes are two different modes of Tz1 bound to a single Tz1 receptor site.

Although $Na_V1.5$ channels showed no negative shift in the voltage dependence of activation upon application of Tz1 (Fig. 2 D), the toxin diminished peak currents without strong use dependence. P_{tox} was estimated to 0.75 ± 0.02 (no prepulse [−pp]) and 0.67 ± 0.03 (prepulse [+pp]; $n = 5$), indicating that $Na_V1.5$ is even more sensitive to Tz1 than $Na_V1.4$. The corresponding ΔV_i value was estimated to 104 ± 8 mV. Inhibition of $Na_V1.5$ activation was characterized by a prepulse-independent maximal P_i value of 0.94 ± 0.08 and a half-maximal concentration of 2.3 ± 0.7 µM without and 3.3 ± 0.9 µM with a prepulse (Fig. 3 B).

Exchange of asparagine for the critical glycine in the background of $Na_V1.4$ (G658N) resulted in a phenotype similar to that of $Na_V1.5$ (Fig. 2 C), although this mutation did not affect the gating parameters under control conditions (Table S1). P_{tox} was 0.85 ± 0.02 (−pp) and 0.86 ± 0.02 (+pp) ($n = 5$), indicating that mutation G658N stabilized toxin interaction compared with wild-type $Na_V1.4$ channels. The corresponding ΔV_i value was estimated to 151 ± 11 mV.

The reverse mutation in the background of $Na_V1.5$ (N803G) conferred a $Na_V1.4$-like toxin phenotype to $Na_V1.5$ (Fig. 2 E). $Na_V1.5$–N803G started activating at about −90 mV in a prepulse-dependent manner because current amplitudes with a prepulse were larger than those without (see current traces at −70 mV in Fig. 2 E). P_{tox} (5 µM Tz1) of this mutant channel was 0.76 ± 0.04 ($n = 5$). Without a prepulse, P_a was 0.26 ± 0.04, and the corresponding ΔV_a was −29.0 ± 1.4 mV. P_i was 0.50 ± 0.05, and the corresponding ΔV_i was 25.9 ± 5.1 mV. This moderate right-shift of the activation only marginally reduced channel open probabilities in the observed voltage range and therefore caused a considerably smaller current inhibition. After a prepulse, no channels were inhibited ($P_i = 0$) and $P_{tox} = P_a$. Conductance–voltage plots obtained from the same experiments describe the Tz1-dependent channel activation in a model-independent manner and are presented in Fig. S2.

The influence of Tz1 on the voltage dependence of steady-state inactivation was analyzed by determining the half-maximal inactivation voltage, V_h, and the corresponding slope factor, k_h, according to Eq. 2 (Fig. S3). Under control conditions, V_h and k_h for $Na_V1.4$ were −73.0 ± 1.8 mV and −5.3 ± 0.2 mV ($n = 7$), respectively. The application of 5 µM Tz1 reduced the maximal current amplitudes to 43.5 ± 2.2% and shifted the V_h by −21.0 ± 4.0 mV without changing k_h. For $Na_V1.5$, 5 µM Tz1 shifted V_h from −96.2 ± 2.6 mV by −4.7 ± 3.2 mV,

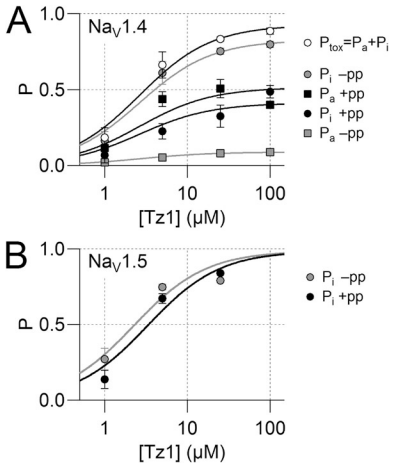

Figure 3. Concentration dependence of Tz1 effects on $Na_V1.4$ and $Na_V1.5$ channels. (A) The estimated probabilities of $Na_V1.4$ channels to be inhibited (P_i) or preactivated (P_a) by Tz1 in the absence (gray symbols; −pp) or presence (black symbols; +pp) of a prepulse as a function of the Tz1 concentration. P_{tox} (open circles) is the sum of P_i and P_a and independent of a prepulse; i.e., P_{tox} is a measure of the fraction of Na_V channels with Tz1 bound. Continuous curves are global data fits according to a Hill equation (Eq. 3). (B) Estimated probabilities for $Na_V1.5$ channels to be inhibited (P_i) by Tz1 versus Tz1 concentration. For data fits in A and B, a Hill coefficient of unity was assumed.

while not changing k_h (−5.5 ± 0.6 mV; $n = 4$); the maximal current amplitude was reduced to 32.3 ± 6.9%. Mutations $Na_V1.4$–G658N and $Na_V1.5$–N803G did not change V_h and k_h ($P >> 0.1$), but current reduction by Tz1 was enhanced for $Na_V1.4$–G658N (reduction to 15 ± 3.0%) and diminished for $Na_V1.5$–N803G (reduction to 94 ± 9%), which is consistent with the notion that Tz1 preferentially suppresses $Na_V1.5$-type channels.

Our previous results (Leipold et al., 2006) revealed that the subtype specificity of Tz1 for Na_V channels is determined by the ss2 pore loop of domain 3. We thus asked if the impact of that domain also affects the inhibitory mode of Tz1 described thus far. We therefore introduced the domain 3 ss2 pore loop of $Na_V1.7$ into $Na_V1.4$ (44p(1.7)4) and $Na_V1.4$–G658N (44p(1.7)4-G658N) and assayed these mutants with respect to Tz1. Independent of a prepulse, in no case did we observe any effect of Tz1, neither left-shift in activation nor current inhibition (Fig. 4 and Fig. S3), strongly suggesting that domain 3 is necessary to stabilize the toxin at the channel protein, whereas the voltage sensor of domain 2 determines the mode of β-toxin effects.

Analysis of mode transitions

The results obtained so far demonstrate that a glycine at position 658 in the domain 2 voltage sensor of $Na_V1.4$ permits a dual function of Tz1 to activate and to inhibit the channels, whereas an asparagine at the equivalent position, such as N803 in $Na_V1.5$, restricts the effect of Tz1 to channel inhibition. To infer about the molecular interpretation of channel "activation" and "inhibition" by Tz1, we measured the unitary current size (i) and the maximal channel open probabilities (P_o) by means of nonstationary noise analysis. Mean currents and ensemble variances of 50–200 individual current responses at various potentials were analyzed for $Na_V1.4$ before and after toxin application (Fig. 5, A and B). Data were best described assuming a constant number of active channels, N, in the absence and presence of Tz1. Tz1 did not affect the single-channel current amplitude (Fig. 5 C, top left) over the whole voltage range. The voltage dependence of P_o (Fig. 5 C, bottom left) was left-shifted by Tz1, consistent with an enhanced activation being the dominant phenotype under this condition. A similar result was obtained for inactivation-deficient channels (Fig. S7). Equivalent experiments were performed for $Na_V1.4$–G658N, $Na_V1.5$, and $Na_V1.5$–N830G, and in no case did Tz1 affect the single-channel current size (Figs. 5 C and S8). For $Na_V1.5$ and $Na_V1.4$–G658N, the most prominent effect of Tz1 was a strong reduction of P_o, whereas the results obtained for $Na_V1.5$–N803G resembled those for $Na_V1.4$. Thus, for channels carrying an asparagine at the critical position, Tz1 stabilizes the resting state, and "channel inhibition" is the sole phenotype.

These results suggest that under certain circumstances, Tz1 may slow down the activation process of Na_V channels by interfering with their voltage sensors in domain 2. True kinetics of Na_V channel activation, however, is not readily accessible because of the overlapping rapid process of inactivation. We therefore analyzed the effects of Tz1 on $Na_V1.4$ and $Na_V1.4$–G658N channels after removal of inactivation. Because Na_V channel mutants with impaired inactivation are difficult to express in mammalian cells, we mutated the inactivation motif of $Na_V1.4$ and $Na_V1.4$–G658N from IFM to IFC (mutation M1305C), still leaving inactivation intact. As illustrated in Fig. 6 (A and B), inactivation is rapidly and efficiently removed from channels with an IFC inactivation motif when the fluorescent dye LY (200 µM), loaded into the cell via the patch pipette, is excited with blue light (Heinemann and Leipold, 2011).

Current–voltage relationships for such inactivation-deficient channels were compiled by measuring the current amplitude 15-ms within the depolarization interval (Fig. 6 C) and analyzed according to Eq. 1. Corresponding current traces are shown in Fig. S5. Without a prepulse, P_{tox} for $Na_V1.4$–IFC was 0.79 ± 0.04 (25 µM Tz1; $n = 5$), P_a was 0.10 ± 0.01, and P_i was 0.69 ± 0.03. The prepulse changed P_a to 0.29 ± 0.01 and P_i to 0.50 ± 0.05. This result demonstrates that loss of fast inactivation has no impact on the qualitative effect of Tz1 on $Na_V1.4$ channels. Current traces from independent experiments in response to 100-ms depolarizations (Fig. 6 E) provide information on the gating kinetics. Without a prepulse, $Na_V1.4$–IFC currents were slightly increased by Tz1 at

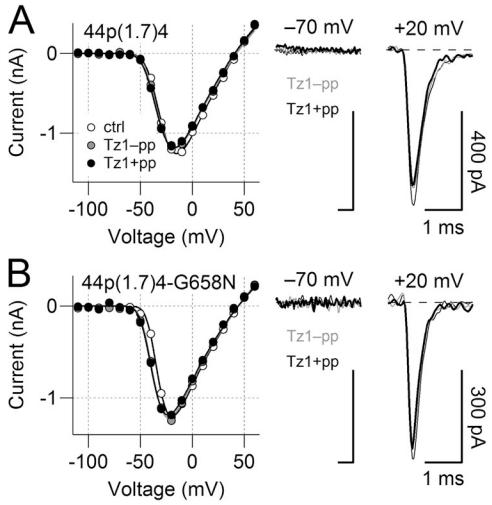

Figure 4. Impact of the domain 3 pore loop on Tz1-induced channel modulation. (A; left) Representative current–voltage plots of 44p(1.7)4 before (open circles) and after the application of 5 µM Tz1 (closed symbols) without (gray) or with (black) a preceding prepulse. Control data are shown without a prepulse, as they are indistinguishable from those with a prepulse. Continuous curves are data fits according to Eq. 1. (Right) Current traces from the same experiments as shown on the left obtained at the indicated potentials in the absence (thin black) and presence of Tz1 without (gray) and with (thick black) a prepulse. (B) Similar experiments as in A for mutant 44p(1.7)4–G658N.

the beginning of the depolarization phase but continued to rise during the depolarization phase, indicating that some fraction of channels undergoes delayed activation under this condition. This situation was reversed when channels were primed with a prepulse. Now Tz1 led to greater increases of current at the beginning of the depolarization phase followed by a decline. Notably, current traces without and with a prepulse seem to approach a common steady state, as one would predict from a model in which Tz1 slows the activation as well as the deactivation kinetics of $Na_V1.4$.

Similar experiments for $Na_V1.4$–IFC–G658N (Figs. 6, D and F, and S5) showed that the noninactivating current of $Na_V1.4$–IFC–G658N in the presence of Tz1 was readily described by P_i of 0.75 ± 0.02 without and 0.83 ± 0.1 with a prepulse (n = 5). Current traces of 100-ms duration (Fig. 6 F) revealed a substantial slowing of activation in the presence of Tz1, albeit without any prepulse dependence. The phenotype "inhibited by Tz1" can be explained by delayed activation; in the presence of normal rapid inactivation, the maximal channel open probability and, hence, the peak current, is effectively reduced.

Coupling to the gating charge of domain 2 voltage sensor

To reveal the impact of the domain 2 voltage sensor on the modes of β-toxin action, we individually mutated the positively charged amino acids in the S4 segment of $Na_V1.4$ domain 2 to cysteines. All mutations resulted in functional channels with gating parameters comparable to those of wild-type $Na_V1.4$, assuring that altered gating properties did not influence subsequent experiments (Figs. 7 A, open symbols, and S6, and Table S1). Exposed to 5 µM Tz1, all gating charge mutants displayed the phenotypes "activated by Tz1" and "inhibited by Tz1." There was no significant effect on the P_{tox} values for R669C, K672C, and K675C, and just a slight increase in P_{tox} for R663C and R666C to 0.86 ± 0.01 (n = 5) and 0.85 ± 0.01 (n = 5), respectively (Fig. 7 B). This can be interpreted in a way that mutations R669C, K672C, and K675C did not much affect the affinity of Tz1 to the channel, whereas mutations R663C and R666C increased it. The corresponding P_{tox}, P_a, and P_i values furthermore show that charge neutralizations either affected the steady-state distribution of P_a and P_i or their use dependence (Fig. 7 B, bottom). Mutation R666C had the greatest impact because it showed almost no use dependence. In addition, it displayed less Tz1-induced left-shift in the voltage dependence of activation (ΔV_a) compared with the wild type and the other mutants (Fig. 7 B, middle). Also indicated in Fig. 7 B (top) are the estimates for the right-shift of those channels inhibited by Tz1 (ΔV_i).

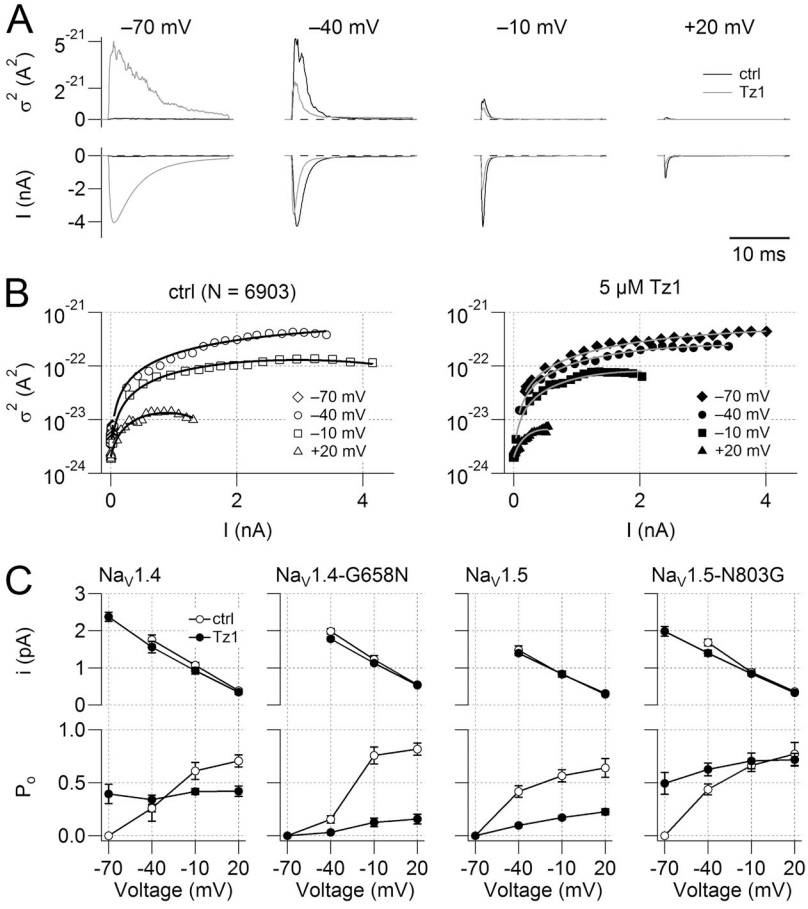

Figure 5. Nonstationary noise analysis of Tz1 effects. (A) Mean current responses of $Na_V1.4$ channels (bottom, I) and their ensemble variances (top, σ^2) from at least 100 individual current traces elicited at the indicated voltages in the absence (black) and presence (gray) of 5 µM Tz1. (B) Variance as a function of mean current for several voltages in the absence (left) and presence (right) of Tz1. Continuous lines are results of global data fits according to Eq. 4. Data fits were constrained as described in Materials and methods. N is the estimate for the number of active channels in this particular experiment. (C) Estimated single-channel current (i) and maximal open probability (P_o) as a function of voltage in the absence (open circles) and presence (closed circles) of Tz1 for the indicated channel types. P_o values at −70 mV were set to zero for all channel variants in the absence of Tz1; for $Na_V1.4$–G658N and $Na_V1.5$, this was also done in the presence of Tz1 because channels are closed under these conditions. Data points, connected by straight lines, are presented as mean ± SEM. The numbers of individual experiments were n = 5, 5, 4, and 5.

To obtain information on the kinetics of toxin-mode transitions, we applied tailored pulse protocols in the presence of 25 µM Tz1. Tz1-dependent activation was induced by a variable conditioning depolarization and subsequently monitored at a test potential of −70 mV, because only toxin-bound channels are active at this potential (Fig. 8 A). For measuring Tz1-dependent deactivation kinetics, channels were first primed with two depolarizing prepulses, followed by a test pulse to −70 mV (I_{max}) to monitor the Tz1-preactivated channels (Fig. 8 B). Subsequently, a variable hyperpolarizing conditioning pulse was applied to induce relaxation

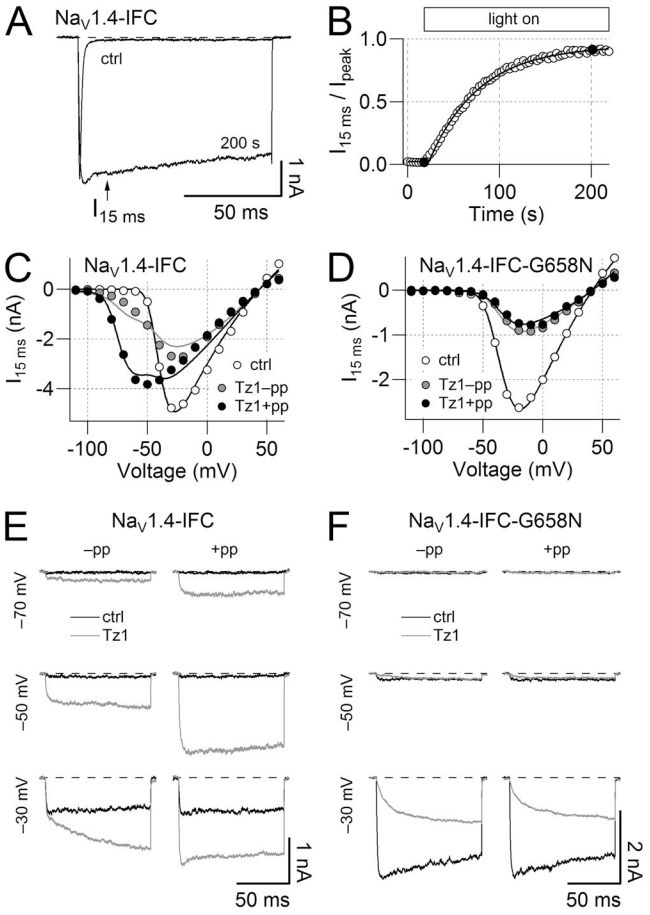

Figure 6. Tz1 effects on inactivation-deficient Na$_V$ channels. (A) Current traces of Na$_V$1.4–IFC channels at −20 mV in the presence of 200 µM of intracellular LY before (ctrl) and 200 s after illumination with blue light. The arrow indicates 15 ms, the time at which the removal of fast inactivation was analyzed. (B) Time course of the loss of fast inactivation of Na$_V$1.4–IFC mutant channels. The ratio of current after 15 ms and the peak current was monitored at an interval of 5 s and plotted as a function of time. The continuous line is a single-exponential description of the data. Closed circles mark the data points obtained from the current traces shown in A. During irradiation, Na$_V$1.4–IFC progressively lost fast inactivation, characterized by a time constant of 79.6 ± 6.4 s; inactivation loss saturated at 89.1 ± 2.2% (n = 6). Na$_V$1.4–IFC–G658N lost inactivation with a time constant of 92.2 ± 12.9 s and saturated at 93.5 ± 2.5% (n = 6). (C and D) Representative current–voltage plots of inactivation-deficient Na$_V$1.4–IFC and the inactivation-deficient double mutant Na$_V$1.4–IFC–G658N in the absence (open circles) and presence (closed symbols) of 25 µM Tz1 without (gray) or with (black) a prepulse. Continuous curves are data fits according to Eq. 1. (E and F) Current traces from independent experiments obtained for 100-ms depolarizations to the indicated voltages in the absence (black) and presence (gray) of 25 µM Tz1 without (−pp) or with (+pp) a prepulse.

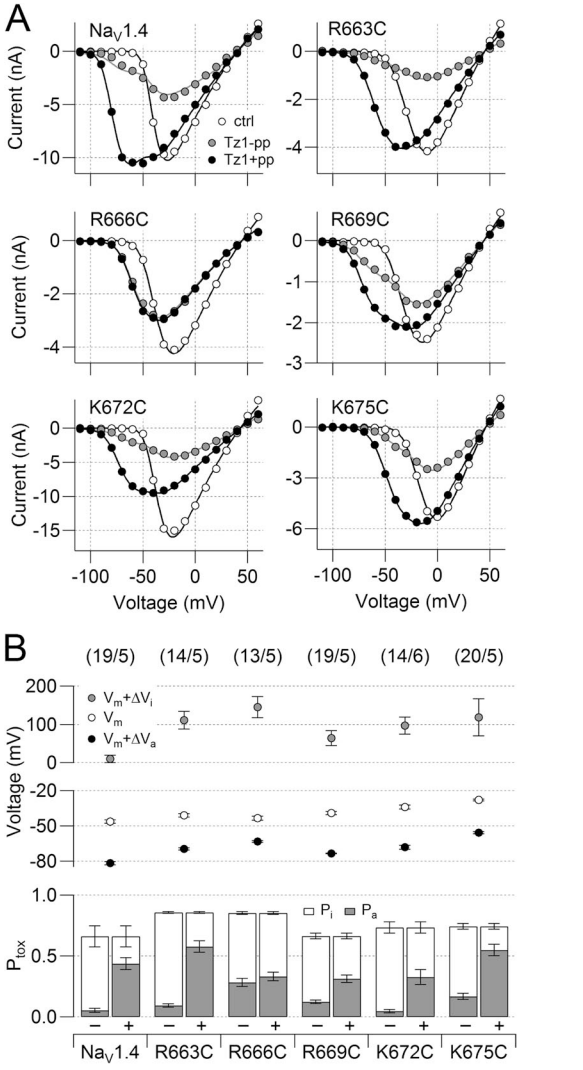

Figure 7. Charge neutralizations in the domain 2 voltage sensor of Na$_V$1.4 differentially influence gating modification by Tz1. (A) Representative current–voltage plots of the indicated Na$_V$1.4 mutant channels in the absence (open circles) and presence (closed circles) of 5 µM Tz1 without (gray) or with (black) a prepulse. Continuous curves are data fits according to Eq. 1. (B; top) Estimates for the half-maximal activation voltages under control conditions (V_m) and for channels activated ($V_m + \Delta V_a$) and inhibited ($V_m + \Delta V_i$) by Tz1 according to data fits with Eq. 1. (Bottom) Probabilities of channels to be preactivated (gray bars; P_a) or inhibited (white bars; P_i) by Tz1 in absence (−) or presence (+) of a prepulse. P_a and P_i values were estimated from current–voltage plots as shown in A. P_{tox}, the probability of channels to be modified by Tz1, is displayed as the sum of P_a and P_i values, i.e., is denoted by the total height of the histogram bars. The number of independent experiments for control conditions and with Tz1, respectively, is indicated in parentheses.

and, finally, the channel fraction not deactivated after conditioning was determined with a second test pulse to −70 mV (I_d). Activation and deactivation kinetics were measured at various conditioning voltages and analyzed as a function of conditioning duration (Fig. 8, C and D). The resulting time constants, plotted as a function of the corresponding conditioning voltages, were described with a voltage-dependent transition-state model (Eq. 6) assuming the states "activated by Tz1" and "inhibited by Tz1" (Fig. 8 E). The charge transfer associated with this process was estimated to an equivalent of 2.4 ± 0.1 elementary charges, where 80% contribute to the activation process and 20% are associated with the deactivation process. From Fig. 8 E, the time constant for sensor movement at −30 mV is estimated to ∼20 ms, a kinetics that matches to the current relaxation of Tz1-occupied $Na_V1.4$–IFC channels shown in Fig. 6 E (∼40 ms). Assuming that Tz1 binding is independent of voltage and the conformational channel state (see Figs. 6 and 7 B), the information obtained with this approach most likely characterizes the Tz1-controlled gating transitions of the domain 2 voltage sensor.

Subjected to the same analysis of Tz1-controlled gating transitions (Fig. S9), all gating charge mutants showed quantitative differences in Tz1-dependent activation and deactivation gating compared with wild-type $Na_V1.4$ channels (Fig. 9 A). The parameters characterizing channel activation and deactivation are summarized in Fig. 9 B. The net gating charge transfer during Tz1-controlled channel activation and deactivation was not much affected by individual charge neutralizations but, interestingly, the mutations differentially affected the gating charge associated with channel activation and deactivation. For example, neutralization of R663 at the outermost end of the domain 2 S4 segment reduced the gating charge associated with channel activation, q_a, from 2.0 ± 0.1 to 1.5 ± 0.1 e_0 and increased the fraction involved in Tz1-dependent deactivation, q_d, from 0.4 ± 0.1 to 0.5 ± 0.1 e_0 (Fig. 9 B), with the consequence of slowed activation and faster deactivation kinetics for R663C (Fig. 9 A). Qualitatively, the opposite was observed for mutation R669C in the center of the S4 segment. The gating charge associated with activation was decreased (q_a = 1.7 ± 0.1 e_0), whereas that for deactivation vanished (q_d = 0), with the result of accelerated activation gating (Fig. 9, A and B). Mutation K672C was without much effect on the gating charge. K675C, at the end of S4, showed a reduction of the activation- and deactivation-associated gating charge (q_a = 1.9 ± 0.1 e_0 and q_d = 0.2 ± 0.1 e_0) and a slowdown of both Tz1-dependent activation and deactivation. Mutation R666C did not show any use dependence, thus precluding the determination of kinetic parameters. Apparently, individual gating charges of the domain 2 S4 segment differentially influence how a scorpion β toxin affects activation and deactivation of that particular voltage sensor.

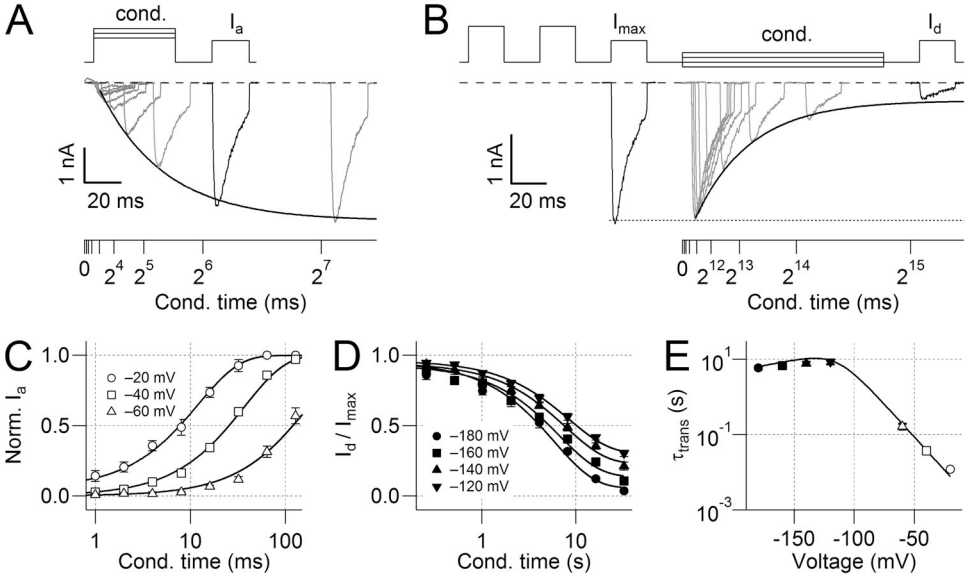

Figure 8. Voltage dependence of Tz1-induced gating modification. (A; top) Protocol used to measure the voltage-dependent preactivation of $Na_V1.4$ channels in the presence of Tz1. (Bottom) Current traces at −70 mV in response to conditioning pulses (here to −40 mV) are shown in gray and are offset in time by the conditioning durations. The current trace corresponding to a conditioning time of 64 ms is highlighted (black). The continuous line is a single-exponential fit to the peak current responses after conditioning, I_a. (B; top) Protocol used to measure the voltage-dependent channel deactivation in the presence of Tz1. (Bottom) Current traces at −70 mV in response to conditioning pulses (here to −160 mV) are shown in gray and are offset in time by the conditioning durations. The current trace corresponding to a conditioning time of 32.768 s is highlighted. The continuous line is a single-exponential fit to the peak current responses after conditioning (I_d) and describes the deactivation of $Na_V1.4$ channels in the presence of toxin. (C) Normalized I_a as a function of the conditioning time, shown for the indicated conditioning voltages with superimposed single-exponential data fits. (D) Normalized I_d as a function of conditioning time, shown for the indicated conditioning voltages with superimposed single-exponential data fits. (E) Time constants of Tz1-induced gating modification in the activation (open symbols) and deactivation (closed symbols) direction as a function of voltage. The continuous line is a data fit according to a transition-state model (Eq. 6) assuming the transfer of q = 2.4 ± 0.1 e_0 with a symmetry factor of δ = 0.21 ± 0.05 (n = 3–5). Tz1 concentration was 25 µM in all panels.

DISCUSSION

Although recent investigations on the molecular mechanism of scorpion β toxins primarily focused on their ability to activate Na_V channels, marked channel inhibition often was neglected. In this study, we assayed both modes of scorpion β-toxin Tz1 on $Na_V1.4$ and $Na_V1.5$ channels in a systematic and quantitative approach, with the aim to elucidate the molecular mechanism underlying the bimodal activity of this toxin.

Tz1 discriminates $Na_V1.4$ and $Na_V1.5$

Tz1 enhanced activation of skeletal muscle $Na_V1.4$ channels at resting membrane potentials, while reducing channel conductance at stronger depolarization. The relative contribution of the two effects displayed a marked use dependence without a noticeable change in toxin–channel association. This result is consistent with a state- and voltage-independent toxin–channel interaction, as proposed for β toxins Cn2 (Jover et al., 1980) and AaIT (Gordon et al., 1984), based on physical binding studies. For the cardiac $Na_V1.5$ channels, Tz1 only reduced Na^+ conductance without use dependence, and no activation at low voltages was observed (Figs. 1 and 2). Channel inhibition as the sole phenotype on $Na_V1.5$ channels was also reported for β toxins Ts1 (Marcotte et al., 1997), CssIV (Cestèle et al., 1998), Lqhβ1 (Gordon et al., 2003), and CssII (Smith et al., 2005), whereas enhanced activation of $Na_V1.5$ by a β toxin has not been described. This suggests that not only Tz1 but also β toxins in general are potential inhibitors of cardiac $Na_V1.5$ channels. Total P_{tox} values resulting from our quantitative data description even revealed that $Na_V1.5$ channels are more sensitive to Tz1 than $Na_V1.4$. This result extends a recent study in which we demonstrated an increased Tz1 susceptibility of a $Na_V1.4$ chimera with the Tz1 specificity–determining epitope of $Na_V1.5$ in the distal pore loop of domain 3 (Leipold et al., 2006), and corroborates that this epitope is the major determinant for the channel's β-toxin specificity. As demonstrated in Fig. 4 using domain 3 pore loop chimeras, this argument also holds for the inhibitory effect of Tz1.

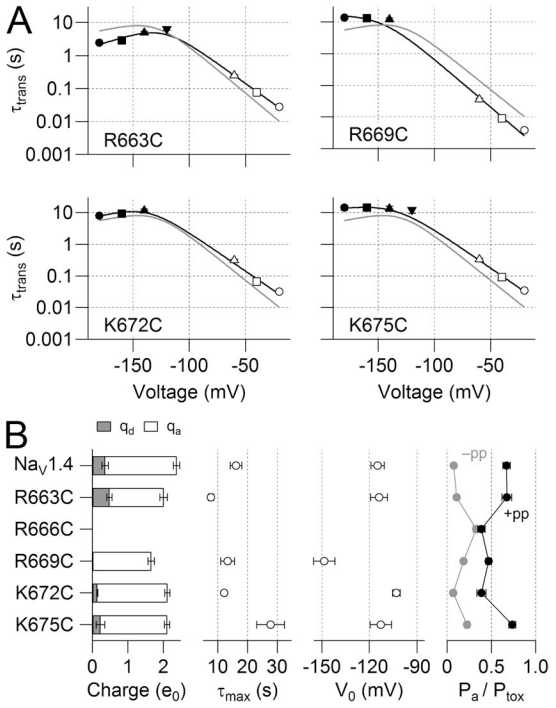

Figure 9. Effect of voltage-sensor mutants on Tz1-induced gating modification. (A) Activation (open symbols) and deactivation (closed symbols) time constants of the indicated $Na_V1.4$ mutant channels in the presence of 25 µM Tz1 were calculated from experiments as shown in Fig. 8 and plotted as a function of voltage (n = 3–8). The continuous lines are data fits according to Eq. 6. The gray line represents data of wild-type $Na_V1.4$. (B) The gating charge involved in voltage-dependent activation (q_a; white bars) and deactivation (q_d; gray bars) in the presence of Tz1 is shown as histogram bars. τ_{max} is the maximal time constant of the transition between the activated and the resting state of the channels, and V_0 is the corresponding equilibrium voltage. Data were calculated from experiments as shown in A. The fractions of channels preactivated in the presence of Tz1 (P_a/P_{tox}) without (gray symbols; −pp) or with (black symbols; +pp) a prepulse were calculated from current–voltage plots to predict functional consequences of Tz1 interaction with wild-type and mutant $Na_V1.4$ channels.

The molecular determinant for how a scorpion β toxin affects Na_V channels appears to reside in the S3/S4 linker in domain 2 (Cestèle et al., 1998, 2006; Zhang et al., 2011). As shown previously by Cestèle et al. (1998) for the effect of CssIV on $Na_V1.2$ and by us for the Tz1 effect on $Na_V1.4$ (Leipold et al., 2006), a single glycine residue at position G658 (numbering for rat $Na_V1.4$) is required for the mode described as channel activation. Activation of cardiac $Na_V1.5$ channels, harboring an asparagine at the homologous position, is not left-shifted by β toxins. This G-to-N exchange only has a minor impact on the toxin–channel interaction per se, but the major effect is an abolition of use-dependent transitions between the modes "activated by Tz1" and "inhibited by Tz1." The lack of a side chain in glycine favors use-dependent transitions among the modes, whereas in the presence of the larger asparagine, "inhibited by Tz1" is the only mode. Considering the different size of Gly and Asn, a strong steric component in the molecular mechanism of Tz1 action appears likely.

Voltage–sensor trapping mechanism

The voltage–sensor trapping model developed by Cestèle et al. (1998) anticipates that both left-shift in activation and reduction of peak current are related to only one toxin interaction site. An alternative model assuming two distinct toxin-binding sites for β toxins, one mediating enhanced activation and another one related to peak current reduction, was also discussed (de la Vega and Possani, 2007). This alternative view is supported by Marcotte et al. (1997); using chimeric $Na_V1.4/1.5$ channels, they concluded that interaction of the β-toxin Ts1 with domain

2 is required for enhanced channel activation but not sufficient to reduce the peak current. Zhu et al. (2009) suggest two binding sites for BmK AS to explain the complex effects based on measurements on Na^+ current endogenous to ND7-23 cells and $Na_V1.2$ in oocytes. Further support for such a two-site model comes from Tsushima et al. (1999), who showed that β-toxin TdVIII did not affect the activation of noninactivating $Na_V1.4$ mutants but reduced the peak current much like in wild-type channels.

Data presented here for Tz1, however, can be explained sufficiently by assuming a single-site model because (a) the two Tz1 phenotypes of $Na_V1.4$ have identical binding constants (Fig. 3 A); (b) both Tz1 phenotypes are bidirectionally conferred by mutating only a single residue (G658N in $Na_V1.4$); and (c) the apparent Tz1 affinity of $Na_V1.4$ is not decreased when the phenotype "activated by Tz1" is eliminated by mutation G658N, as one would predict if both phenotypes correspond to independent binding sites. Moreover, as pointed out in Fig. 4, the activity of the toxin as such is largely determined by the pore loop of domain 3. If that domain is incompatible, no typical β-toxin effect is observed anymore, indicating that the affinity of the S3/S4 linker of domain 2 alone is not sufficient to support a firm channel–toxin interaction. Thus, a likely scenario is that the toxin is stabilized at the channel surface by many physical interactions (the one to the domain 3 pore loop apparently is an important one), but, once in this position, it additionally interferes with the movement of the domain 2 voltage sensor.

This interference manifests itself as an apparent left-shift in the voltage dependence of activation for those channels being activated by Tz1 and a substantial right-shift for channels being inhibited by Tz1 (Eq. 1). Compatible with this conclusion, nonstationary noise analysis revealed that the single-channel conductance remained constant upon Tz1 application, whereas the maximal open probabilities were affected depending on channel type and mode of toxin action (Figs. 5, S7, and S8). A similar result was obtained by Yatani et al. (1988), who showed that Ts1 inhibited endogenous Na^+ currents in rat neonatal heart cells by reducing the open probability without changing the single-channel current amplitude.

Although a left-shift in voltage dependence of channel activation at least qualitatively can be explained by locking a voltage sensor in the activated position, the molecular interpretation of "channel inhibition" is not readily apparent. Transition of toxin-occupied channels into closed-state inactivation as the primary cause of current reduction could be dismissed based on experiments using inactivation-deficient Na_V channels. Upon inactivation removal of $Na_V1.4$–IFC and $Na_V1.4$–IFC–G658N with photo-activated LY (Fig. 6), channels retained their dependence on Tz1. Furthermore, use-dependent transitions between the modes of Tz1 action could be directly observed for $Na_V1.4$–IFC when unmasked from rapid inactivation (Fig. 6 E) but not for $Na_V1.4$–IFC–G658N (Fig. 6 F). Therefore, peak current inhibition of $Na_V1.4$ by Tz1 is a result of slowed activation combined with unaltered fast inactivation, thus leading to a strongly reduced maximal open probability. This mechanism seems to be facilitated in $Na_V1.4$–IFC–G658N because these channels activated much slower in the presence of Tz1 compared with $Na_V1.4$–IFC. Our results for noninactivating $Na_V1.4$–IFC channels stay in marked contrast to an earlier report by Tsushima et al. (1999) in which mutagenesis-based removal of inactivation in $Na_V1.4$ channels eliminated the left-shifting potency of β-toxin TdVIII, albeit retaining channel inhibition. At present, we cannot provide an obvious explanation for this apparent difference other than that the molecular mechanism underlying TdVIII action may differ from those of other β toxins.

Our data are best described by a model in which Tz1 binds to $Na_V1.4$ channels independent of the channel's conformational state. In the presence of Tz1, the energy barrier separating deactivated and activated states for the domain 2 voltage sensor is increased, thus slowing down sensor movements in both directions. Starting from the deactivated state after long hyperpolarization episodes, Tz1-occupied channels activate more slowly and, hence, only a few channels manage to activate before entering the inactivated state. Once in an activated state, the sensor deactivates very slowly, such that in subsequent depolarizing pulses the sensor is already activated, thus leading to higher open probabilities.

Individual neutralization of the charged residues in domain 2 S4 revealed that all charges affect Tz1-dependent gating transitions, but the most noticeable effects were observed for the three outermost gating charges. In the presence of Tz1, R663C displayed slower activation and faster deactivation gating compared with wild-type channels, highlighting a dominant role of this charge in voltage-sensor activation. Qualitatively, the opposite effect was observed for R669C in the center of the sensor, indicating its involvement in sensor deactivation. R666C in the second outermost position eliminated the use independence of Tz1 effects as if it would strongly increase the energy barrier between both states of the voltage sensor. A similar role of the second outermost arginine for the action of CssIV was also demonstrated for $Na_V1.2$ channels (Cestèle et al., 2001).

Despite the compelling evidence that the domain 2 voltage sensor plays a crucial role in β-toxin action, it is quite evident that an immobilization of that sensor alone will not result in marked left-shifts in voltage dependence of activation. This was nicely demonstrated by Campos et al. (2007), who showed with voltage-clamp fluorometry in the presence of Ts1 that this β toxin impairs the movement of all sensors. Only by means of the strong coupling among the voltage sensors in domains 1–3 is a concerted β toxin–induced augmentation of channel opening at resting voltages conceivable. Interestingly, even in very

simple activation models of Na_V channels, such as the classical Hodgkin–Huxley formalism (Eq. 1), locking of a single voltage sensor in the "off" position should have a profound effect on channel activation and should effectively right-shift the voltage dependence of channel opening. Thus, using fluorimetric methods and Tz1 applied to $Na_V1.5$ channels might be suited to test for a potential cooperativity of voltage-sensor movements in the deactivating direction.

Na_V channel inhibition via a gating modification mechanism is not unique to scorpion β toxins, as demonstrated for the ceratoxins CcoTx1, CcoTx2, and CcoTx3 (*Ceratogyrus cornuatus*) and PaurTx3 (*Phrixotrichus auratus*) (Bosmans et al., 2006). These tarantula peptides inhibit Na_V channels by shifting their voltage dependence of activation to more positive voltages, suggesting a voltage–sensor mechanism of toxin action. Moreover, channel inhibition by an interaction with the voltage sensors in domain 2 was demonstrated for tarantula toxin ProTox II from *Thrixopelma pruriens* (Sokolov et al., 2008) and for the structurally unrelated μO conotoxin MrVIA (*Conus marmoreus*; Leipold et al., 2007). Both peptides "block" Na_V channels by stabilizing the resting state of the channels' voltage sensors in domain 2, albeit without the bimodal function of scorpion β toxins.

Excitatory and depressant modes of Tz1

Several studies described the physiological impact of β toxins in mammals and insects and highlighted their excitatory and/or depressant activity (e.g., Gordon et al., 1992, 2003; Cohen et al., 2007; Karbat et al., 2010). Excitatory β toxins lead to a fast contraction paralysis, whereas depressant β toxins cause a progressive flaccid paralysis. The molecular details of such different physiological consequences are not unambiguously known. The data presented here for Tz1 suggest that the physiological correlates to "excitatory" and "depressant" are most likely a combination of channel subtype specificity and, more importantly, the mode of toxin action strongly determined by electrical activity of the afflicted neuronal cell. Particularly stimulated by recent results assigning antinociceptic potencies to scorpion toxins (e.g., Liu et al., 2008), the exploration of the pharmacological potential of scorpion β toxins or peptides with a similar activity profile will be important. Besides identifying the molecular determinants for the toxins' channel specificity, it will be a challenge to rationally control β-toxin modes as to deliberately elicit physiologically excitatory or inhibitory responses.

This work was supported by the Deutsche Forschungsgemeinschaft (HE 2993/5-2 to S.H. Heinemann) and FONACIT-CNPq (PI-20040000385 to A. Borges).

Kenton J. Swartz served as editor.

Submitted: 15 September 2011
Accepted: 5 March 2012

REFERENCES

Bai, Z.T., T. Liu, X.Y. Pang, Z.F. Chai, and Y.H. Ji. 2007. Suppression by intrathecal BmK IT2 on rat spontaneous pain behaviors and spinal c-Fos expression induced by formalin. *Brain Res. Bull.* 73:248–253. http://dx.doi.org/10.1016/j.brainresbull.2007.03.007

Borges, A., M.J. Alfonzo, C.C. García, N.J. Winand, E. Leipold, and S.H. Heinemann. 2004. Isolation, molecular cloning and functional characterization of a novel β-toxin from the Venezuelan scorpion, *Tityus zulianus*. *Toxicon.* 43:671–684. http://dx.doi.org/10.1016/j.toxicon.2004.02.022

Bosmans, F., M.F. Martin-Eauclaire, and J. Tytgat. 2005. The depressant scorpion neurotoxin $LqqIT_2$ selectively modulates the insect voltage-gated sodium channel. *Toxicon.* 45:501–507. http://dx.doi.org/10.1016/j.toxicon.2004.12.010

Bosmans, F., L. Rash, S. Zhu, S. Diochot, M. Lazdunski, P. Escoubas, and J. Tytgat. 2006. Four novel tarantula toxins as selective modulators of voltage-gated sodium channel subtypes. *Mol. Pharmacol.* 69:419–429. http://dx.doi.org/10.1124/mol.105.015941

Campos, F.V., B. Chanda, P.S.L. Beirão, and F. Bezanilla. 2007. β-Scorpion toxin modifies gating transitions in all four voltage sensors of the sodium channel. *J. Gen. Physiol.* 130:257–268. http://dx.doi.org/10.1085/jgp.200609719

Catterall, W.A. 2000. From ionic currents to molecular mechanisms: the structure and function of voltage-gated sodium channels. *Neuron.* 26:13–25. http://dx.doi.org/10.1016/S0896-6273(00)81133-2

Catterall, W.A., V. Trainer, and D.G. Baden. 1992. Molecular properties of the sodium channel: a receptor for multiple neurotoxins. *Bull. Soc. Pathol. Exot.* 85:481–485.

Catterall, W.A., S. Cestèle, V. Yarov-Yarovoy, F.H. Yu, K. Konoki, and T. Scheuer. 2007. Voltage-gated ion channels and gating modifier toxins. *Toxicon.* 49:124–141. http://dx.doi.org/10.1016/j.toxicon.2006.09.022

Cestèle, S., Y. Qu, J.C. Rogers, H. Rochat, T. Scheuer, and W.A. Catterall. 1998. Voltage sensor-trapping: enhanced activation of sodium channels by beta-scorpion toxin bound to the S3-S4 loop in domain II. *Neuron.* 21:919–931. http://dx.doi.org/10.1016/S0896-6273(00)80606-6

Cestèle, S., T. Scheuer, M. Mantegazza, H. Rochat, and W.A. Catterall. 2001. Neutralization of gating charges in domain II of the sodium channel α subunit enhances voltage-sensor trapping by a β-scorpion toxin. *J. Gen. Physiol.* 118:291–302. http://dx.doi.org/10.1085/jgp.118.3.291

Cestèle, S., V. Yarov-Yarovoy, Y. Qu, F. Sampieri, T. Scheuer, and W.A. Catterall. 2006. Structure and function of the voltage sensor of sodium channels probed by a beta-scorpion toxin. *J. Biol. Chem.* 281:21332–21344. http://dx.doi.org/10.1074/jbc.M603814200

Cha, A., P.C. Ruben, A.L. George Jr., E. Fujimoto, and F. Bezanilla. 1999. Voltage sensors in domains III and IV, but not I and II, are immobilized by Na^+ channel fast inactivation. *Neuron.* 22:73–87. http://dx.doi.org/10.1016/S0896-6273(00)80680-7

Chen, B., and Y. Ji. 2002. Antihyperalgesia effect of BmK AS, a scorpion toxin, in rat by intraplantar injection. *Brain Res.* 952:322–326. http://dx.doi.org/10.1016/S0006-8993(02)03241-9

Chen, H., D. Gordon, and S.H. Heinemann. 2000. Modulation of cloned skeletal muscle sodium channels by the scorpion toxins Lqh II, Lqh III, and Lqh alphaIT. *Pflugers Arch.* 439:423–432. http://dx.doi.org/10.1007/s004240050959

Chen, J., X.H. Feng, J. Shi, Z.Y. Tan, Z.T. Bai, T. Liu, and Y.H. Ji. 2006. The anti-nociceptive effect of BmK AS, a scorpion active polypeptide, and the possible mechanism on specifically modulating voltage-gated Na^+ currents in primary afferent neurons. *Peptides.* 27:2182–2192. http://dx.doi.org/10.1016/j.peptides.2006.03.026

Cohen, L., Y. Troub, M. Turkov, N. Gilles, N. Ilan, M. Benveniste, D. Gordon, and M. Gurevitz. 2007. Mammalian skeletal muscle voltage-gated sodium channels are affected by scorpion depressant

"insect-selective" toxins when preconditioned. *Mol. Pharmacol.* 72: 1220–1227. http://dx.doi.org/10.1124/mol.107.039057

de la Vega, R.C., and L.D. Possani. 2007. Novel paradigms on scorpion toxins that affects the activating mechanism of sodium channels. *Toxicon.* 49:171–180. http://dx.doi.org/10.1016/j.toxicon.2006.09.016

DeCaen, P.G., V. Yarov-Yarovoy, Y. Zhao, T. Scheuer, and W.A. Catterall. 2008. Disulfide locking a sodium channel voltage sensor reveals ion pair formation during activation. *Proc. Natl. Acad. Sci. USA.* 105:15142–15147. http://dx.doi.org/10.1073/pnas.0806486105

Gellens, M.E., A.L. George Jr., L.Q. Chen, M. Chahine, R. Horn, R.L. Barchi, and R.G. Kallen. 1992. Primary structure and functional expression of the human cardiac tetrodotoxin-insensitive voltage-dependent sodium channel. *Proc. Natl. Acad. Sci. USA.* 89: 554–558. http://dx.doi.org/10.1073/pnas.89.2.554

Gordon, D. 1997. Sodium channels as targets for neurotoxins: mode of action and interaction of neurotoxins with receptor sites on sodium channels. *In* Toxins And Signal Transduction. Y. Gutman and P. Lazarowici, editors. Harwood Academic Publishers, Netherlands. 119–149.

Gordon, D., E. Jover, F. Couraud, and E. Zlotkin. 1984. The binding of an insect selective neurotoxin (AaIT) from scorpion venom to locust synaptosomal membranes. *Biochim. Biophys. Acta.* 778:349–358. http://dx.doi.org/10.1016/0005-2736(84)90379-1

Gordon, D., H. Moskowitz, M. Eitan, C. Warner, W.A. Catterall, and E. Zlotkin. 1992. Localization of receptor sites for insect-selective toxins on sodium channels by site-directed antibodies. *Biochemistry.* 31:7622–7628. http://dx.doi.org/10.1021/bi00148a025

Gordon, D., N. Ilan, N. Zilberberg, N. Gilles, D. Urbach, L. Cohen, I. Karbat, O. Froy, A. Gaathon, R.G. Kallen, et al. 2003. An 'Old World' scorpion beta-toxin that recognizes both insect and mammalian sodium channels. *Eur. J. Biochem.* 270:2663–2670. http://dx.doi.org/10.1046/j.1432-1033.2003.03643.x

Guan, R., C.G. Wang, M. Wang, and D.C. Wang. 2001. A depressant insect toxin with a novel analgesic effect from scorpion *Buthus martensii Karsch. Biochim. Biophys. Acta.* 1549:9–18. http://dx.doi.org/10.1016/S0167-4838(01)00241-2

Heinemann, S.H., and E. Leipold. 2011. Tools for studying peptide toxin modulation of voltage-gated sodium channels. *In* Toxins and Ion Transfers, SFET Editions. http://sfet.asso.fr/international/images/stories/SFET/pdf/Ebook-RT19-2011-signets.pdf (accessed 12 March 2012).

Heinemann, S.H., H. Terlau, W. Stühmer, K. Imoto, and S. Numa. 1992. Calcium channel characteristics conferred on the sodium channel by single mutations. *Nature.* 356:441–443. http://dx.doi.org/10.1038/356441a0

Jover, E., F. Couraud, and H. Rochat. 1980. Two types of scorpion neurotoxins characterized by their binding to two separate receptor sites on rat brain synaptosomes. *Biochem. Biophys. Res. Commun.* 95:1607–1614. http://dx.doi.org/10.1016/S0006-291X(80)80082-9

Karbat, I., N. Ilan, J.Z. Zhang, L. Cohen, R. Kahn, M. Benveniste, T. Scheuer, W.A. Catterall, D. Gordon, and M. Gurevitz. 2010. Partial agonist and antagonist activities of a mutant scorpion beta-toxin on sodium channels. *J. Biol. Chem.* 285:30531–30538. http://dx.doi.org/10.1074/jbc.M110.150888

Leipold, E., A. Hansel, A. Borges, and S.H. Heinemann. 2006. Subtype specificity of scorpion β-toxin Tz1 interaction with voltage-gated sodium channels is determined by the pore loop of domain 3. *Mol. Pharmacol.* 70:340–347.

Leipold, E., H. DeBie, S. Zorn, A. Borges, B.M. Olivera, H. Terlau, and S.H. Heinemann. 2007. μO conotoxins inhibit Na_V channels by interfering with their voltage sensors in domain-2. *Channels (Austin).* 1:253–262.

Li, Y.J., Z.Y. Tan, and Y.H. Ji. 2000. The binding of BmK IT2, a depressant insect-selective scorpion toxin on mammal and insect sodium channels. *Neurosci. Res.* 38:257–264. http://dx.doi.org/10.1016/S0168-0102(00)00164-4

Liu, T., X.Y. Pang, F. Jiang, Z.T. Bai, and Y.H. Ji. 2008. Anti-nociceptive effects induced by intrathecal injection of BmK AS, a polypeptide from the venom of Chinese-scorpion *Buthus martensi Karsch*, in rat formalin test. *J. Ethnopharmacol.* 117:332–338. http://dx.doi.org/10.1016/j.jep.2008.02.003

Loret, E.P., P. Mansuelle, H. Rochat, and C. Granier. 1990. Neurotoxins active on insects: amino acid sequences, chemical modifications, and secondary structure estimation by circular dichroism of toxins from the scorpion Androctonus australis Hector. *Biochemistry.* 29:1492–1501. http://dx.doi.org/10.1021/bi00458a021

Mantegazza, M., and S. Cestèle. 2005. Beta-scorpion toxin effects suggest electrostatic interactions in domain II of voltage-dependent sodium channels. *J. Physiol.* 568:13–30. http://dx.doi.org/10.1113/jphysiol.2005.093484

Marcotte, P., L.Q. Chen, R.G. Kallen, and M. Chahine. 1997. Effects of *Tityus serrulatus* scorpion toxin gamma on voltage-gated Na^+ channels. *Circ. Res.* 80:363–369.

Oren, D.A., O. Froy, E. Amit, N. Kleinberger-Doron, M. Gurevitz, and B. Shaanan. 1998. An excitatory scorpion toxin with a distinctive feature: an additional alpha helix at the C terminus and its implications for interaction with insect sodium channels. *Structure.* 6:1095–1103. http://dx.doi.org/10.1016/S0969-2126(98)00111-7

Sigworth, F.J. 1977. Sodium channels in nerve apparently have two conductance states. *Nature.* 270:265–267. http://dx.doi.org/10.1038/270265a0

Smith, J.J., S. Alphy, A.L. Seibert, and K.M. Blumenthal. 2005. Differential phospholipid binding by site 3 and site 4 toxins. Implications for structural variability between voltage-sensitive sodium channel domains. *J. Biol. Chem.* 280:11127–11133. http://dx.doi.org/10.1074/jbc.M412552200

Sokolov, S., R.L. Kraus, T. Scheuer, and W.A. Catterall. 2008. Inhibition of sodium channel gating by trapping the domain II voltage sensor with protoxin II. *Mol. Pharmacol.* 73:1020–1028. http://dx.doi.org/10.1124/mol.107.041046

Starkus, J.G., Z. Varga, R. Schönherr, and S.H. Heinemann. 2003. Mechanisms of the inhibition of Shaker potassium channels by protons. *Pflugers Arch.* 447:44–54. http://dx.doi.org/10.1007/s00424-003-1121-0

Tan, Z.Y., X. Mao, H. Xiao, Z.Q. Zhao, and Y.H. Ji. 2001a. *Buthus martensi Karsch* agonist of skeletal-muscle RyR-1, a scorpion active polypeptide: antinociceptive effect on rat peripheral nervous system and spinal cord, and inhibition of voltage-gated Na^+ currents in dorsal root ganglion neurons. *Neurosci. Lett.* 297:65–68. http://dx.doi.org/10.1016/S0304-3940(00)01642-6

Tan, Z.Y., H. Xiao, X. Mao, C.Y. Wang, Z.Q. Zhao, and Y.H. Ji. 2001b. The inhibitory effects of BmK IT2, a scorpion neurotoxin on rat nociceptive flexion reflex and a possible mechanism for modulating voltage-gated Na^+ channels. *Neuropharmacology.* 40:352–357. http://dx.doi.org/10.1016/S0028-3908(00)00168-4

Trimmer, J.S., S.S. Cooperman, S.A. Tomiko, J.Y. Zhou, S.M. Crean, M.B. Boyle, R.G. Kallen, Z.H. Sheng, R.L. Barchi, F.J. Sigworth, et al. 1989. Primary structure and functional expression of a mammalian skeletal muscle sodium channel. *Neuron.* 3:33–49. http://dx.doi.org/10.1016/0896-6273(89)90113-X

Tsushima, R.G., A. Borges, and P.H. Backx. 1999. Inactivated state dependence of sodium channel modulation by β-scorpion toxin. *Pflugers Arch.* 437:661–668. http://dx.doi.org/10.1007/s004240050830

Vandendriessche, T., T. Olamendi-Portugal, F.Z. Zamudio, L.D. Possani, and J. Tytgat. 2010. Isolation and characterization of two novel scorpion toxins: The alpha-toxin-like CeII8, specific for $Na_v1.7$ channels and the classical anti-mammalian CeII9, specific for $Na_v1.4$ channels. *Toxicon.* 56:613–623. http://dx.doi.org/10.1016/j.toxicon.2010.06.008

Wang, C.Y., Z.Y. Tan, B. Chen, Z.Q. Zhao, and Y.H. Ji. 2000. Antihyperalgesia effect of BmK IT2, a depressant insect-selective scorpion toxin in rat by peripheral administration. *Brain Res. Bull.* 53:335–338. http://dx.doi.org/10.1016/S0361-9230(00)00355-5

Yang, N., and R. Horn. 1995. Evidence for voltage-dependent S4 movement in sodium channels. *Neuron.* 15:213–218. http://dx.doi.org/10.1016/0896-6273(95)90078-0

Yang, N., A.L. George Jr., and R. Horn. 1996. Molecular basis of charge movement in voltage-gated sodium channels. *Neuron.* 16:113–122. http://dx.doi.org/10.1016/S0896-6273(00)80028-8

Yang, N., A.L. George Jr., and R. Horn. 1997. Probing the outer vestibule of a sodium channel voltage sensor. *Biophys. J.* 73:2260–2268. http://dx.doi.org/10.1016/S0006-3495(97)78258-4

Yatani, A., G.E. Kirsch, L.D. Possani, and A.M. Brown. 1988. Effects of New World scorpion toxins on single-channel and whole cell cardiac sodium currents. *Am. J. Physiol.* 254:H443–H451.

Zhang, J.Z., V. Yarov-Yarovoy, T. Scheuer, I. Karbat, L. Cohen, D. Gordon, M. Gurevitz, and W.A. Catterall. 2011. Structure-function map of the receptor site for β-scorpion toxins in domain II of voltage-gated sodium channels. *J. Biol. Chem.* 286:33641–33651. http://dx.doi.org/10.1074/jbc.M111.282509

Zhang, X.Y., Z.T. Bai, Z.F. Chai, J.W. Zhang, Y. Liu, and Y.H. Ji. 2003. Suppressive effects of BmK IT2 on nociceptive behavior and c-Fos expression in spinal cord induced by formalin. *J. Neurosci. Res.* 74:167–173. http://dx.doi.org/10.1002/jnr.10723

Zhu, M.M., J. Tao, M. Tan, H.T. Yang, and Y.H. Ji. 2009. U-shaped dose-dependent effects of BmK AS, a unique scorpion polypeptide toxin, on voltage-gated sodium channels. *Br. J. Pharmacol.* 158:1895–1903. http://dx.doi.org/10.1111/j.1476-5381.2009.00471.x

Zlotkin, E., D. Kadouri, D. Gordon, M. Pelhate, M.F. Martin, and H. Rochat. 1985. An excitatory and a depressant insect toxin from scorpion venom both affect sodium conductance and possess a common binding site. *Arch. Biochem. Biophys.* 240:877–887. http://dx.doi.org/10.1016/0003-9861(85)90098-0

Zlotkin, E., M. Gurevitz, E. Fowler, and M.E. Adams. 1993. Depressant insect selective neurotoxins from scorpion venom: chemistry, action, and gene cloning. *Arch. Insect Biochem. Physiol.* 22:55–73. http://dx.doi.org/10.1002/arch.940220107